Ultrasonics 93 (2019) 7–17

Contents lists available at ScienceDirect

Ultrasonics

journal homepage: www.elsevier.com/locate/ultras

Towards quantitative quasi-static ultrasound elastography using a reference layer for liver imaging application: A preliminary assessment

Sathiyamoorthy Selladurai, Arun K. Thittai*

Biomedical Ultrasound Laboratory, Department of Applied Mechanics, Indian Institute of Technology Madras, Chennai, India

ARTICLE INFO

Keywords:
Elastic properties
Quantitative elastography
Reference layer
Strain ratio
Ultrasound

ABSTRACT

Changes in tissue elasticity are generally correlated with pathological phenomena. For example, diffuse liver disease progressively reduces the elasticity of the liver. Quasi-static elastography is popular in clinical applications to visualize regions with different relative stiffness. However, the limitation of this technique is that it provides only qualitative information. To overcome this, we investigate the use of a calibrated reference layer, sandwiched between the transducer and the tissue surface, to quantitatively image the unknown modulus of the examined tissue. The performance of the method was studied through simulations and experiments on agar-gelatin phantoms having Young's modulus within a range appropriate for the liver application. Furthermore, we explored the translational capability of the proposed method to work with existing commercially-available ultrasound scanners having elastography option. The Young's modulus value of the phantom estimated from quantitative elastography in simulation and experiment was compared against the corresponding ground-truth modulus value obtained from COMSOL and Universal Testing Machine (UTM) results, respectively. The results obtained for the compressive elastic modulus of the underlying phantom using quasi-static ultrasound elastography was found to be within 6% and 11% in simulation and experiments, respectively, to the corresponding ground-truth values.

1. Introduction

Manual palpation of tissue has been used by clinicians for centuries to aid in clinical diagnosis. The clinical popularity of manual palpation is due to the fact that pathologic changes in the tissue are generally well-correlated to signs of diseases in organs such as the breast, liver, and prostate. For example, Liver tissue with cirrhosis is known to be significantly stiffer than normal healthy liver tissue [13]. However, manual palpation is generally limited to superficial structures and the diagnosis depends largely on the ability of the physician performing the examination, especially in the tissue like liver, since it is located deeper from the surface of the body.

Accurate assessment of the degree of liver fibrosis is important for the correct diagnosis of liver disease and deciding on an appropriate course of treatment [23]. Liver biopsy is considered the gold standard in determining the degree of liver fibrosis, which helps in the prognosis of the disease condition and guides treatment decisions in the case of the chronic liver disease. The different levels of fibrosis are assessed based on histological/fibrosis scores classified as F0 (no fibrosis), F1 (mild fibrosis), F2 (clinically significant fibrosis), F3 (severe fibrosis) and F4 (cirrhosis), based on revised clinical practice guidelines for liver cirrhosis [44], and grading and staging of liver diseases [39,15]. Unfortunately, liver biopsies are invasive and carry inherent risks of bleeding, infection, and potential sampling error. However, it is found that the different stages of fibrosis also exhibit a good correlation with the stiffness of the liver [7,35]. Recently, the diagnosis of Non-Alcoholic Fatty Liver Disease (NAFLD) is gaining much attention. NAFLD is a disease condition in which the liver stiffens homogenously as the disease progresses [43]. According to the most recent epidemiological studies, the prevalence of NAFLD is 25% globally [4]. Early diagnosis can lead to reversing the disease condition and avoid liver transplant. Therefore, there is a lot of active research towards the development of non-invasive techniques for assessment of liver diseases based on changes in liver stiffness.

In this regard, ultrasound elastography approaches seem to be very promising and are finding its way into clinical use [11]. Some of these techniques provide quantitative values, while others provide qualitative information. The quantitative methods include Transient Elastography (TE) and Shear Wave Elastography (SWE).

The most extensively used and tested method for evaluation of liver fibrosis and staging is transient elastography (TE). Transient elastography, which does not produce images, consists of two parts: a

* Corresponding author at: Biomedical Ultrasound Laboratory, Department of Applied Mechanics, Indian Institute of Technology Madras, Chennai 600036, India.
E-mail address: akthittai@iitm.ac.in (A.K. Thittai).

https://doi.org/10.1016/j.ultras.2018.10.007
Received 12 May 2018; Received in revised form 17 September 2018; Accepted 16 October 2018
Available online 17 October 2018
0041-624X/

mechanical vibrator and a single-channel US transducer. The mechanical vibrator generates a low-frequency shear wave at (50–500) Hz in the target tissue (liver), and the pulse-echo ultrasound acquisitions are used to follow the propagation of the shear wave to measure its speed, C_s[m/s]. The corresponding Young's modulus E [kPa] is computed by $E = 3\ \rho C_s^2$ where, ρ is density of tissue [40]. The disadvantage of this method is that it does not provide a B-mode image that is essential for accurate targeting, it cannot be performed on liver with ascites and it is not coupled with standard ultrasound machine [14].

On the other hand, SWE-based approaches provide a stiffness image only over a smaller region of interest (ROI), yet the clinical experiences and evidence are promising. However, this method will require a dedicated high-end scanner, which may make it expensive for routine scanning in rural, resource-poor regions within developing or underdeveloped countries [26,5]. In contrast, Quasi-static elastography or Real-Time Elastography (RTE) is shown to be feasible even with affordable low-cost scanners [37]. However, RTE provides only qualitative information in the form of relative strain distribution within a region and is more popular in clinical applications where a local contrast is expected (e.g., breast lesion imaging). Therefore, it may be worthwhile to explore approaches to make quasi-static a quantitative method, and thereby make it more suitable for non-invasive liver disease diagnostics. It is of interest to note that in a similar vein quantitative elastography was explored for measuring the degeneration of achilles tendon recently [47], which uses built-in reference layer and strain ratio metric for quantitative measurements.

Few other *in vivo* studies have shown that the quantitative measurements can be made using the quasi-static elastography method. For example, [20] developed a reference material that allows calculating the approximate value of Young's modulus of uterine cervix using quasi-static elastography [20,19]. The Young's modulus of the cervical lip was calculated by multiplying strain ratio with Young's modulus of the custom-made cap (acts as a reference layer). The strain ratio was estimated between the ROI from the cervix and the cap. In another study, [9] reported *in vivo* estimation of elastic properties of the perineum using quasi-static elastography in nulliparous women [9]. Recently, [18] investigated the usefulness of strain images acquired while having a calibrated reference gel-pad in between the transducer and skin in staging lymphedema. However, the above methods although interesting are not directly applicable for liver elastography application as they suffer from the use of non-standard reference layer and do not incorporate contrast transfer efficiency while estimating modulus from strain contrast. The use of contrast transfer efficiency may be important for Young's modulus value estimation of the liver as there appears to be a modulus range-scale that is correlated to the disease stage, and therefore, requires more accuracy [14].

In this study, we explore the use of commercially available gel pad as a standard reference layer to make Quasi-static elastography quantitative for liver imaging. Further, we incorporate the contrast transfer efficiency factor while estimating Young's modulus value of the target tissue. The objectives of this work were

1. To establish and characterize a commercially available gel pad as a potential reference layer.
2. To develop a method for estimating the elastic modulus of an underlying homogeneous tissue using a calibrated reference layer.
3. To assess the translational capability of the proposed method to work with existing commercially-available ultrasound scanner having elastography option.

The feasibility of this overall approach is demonstrated using simulations and *in vitro* experiments.

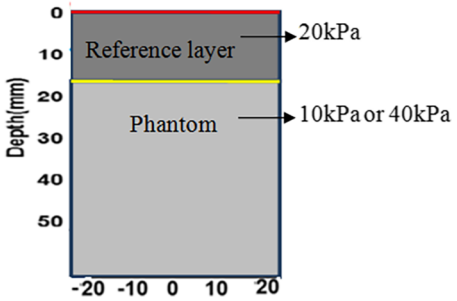

Fig. 1. A schematic of FEM model with reference layer placed above the phantom.

2. Materials and methods

2.1. Simulations

The simulation comprised of two main components, (1) Finite-element simulation of 2D plane-strain model, and (2) Ultrasound simulation of pre- and post-compression ultrasound RF data.

2.1.1. Finite element simulation

A 2D plane-strain model was built using Finite Element Method (FEM) software (COMSOL$^{(R)}$, AB, Stockholm, Sweden). The geometry consisted of a homogeneous medium with overall dimensions of 40 mm × 40 mm. A reference layer of 40 mm × 20 mm (width × height) having 20 KPa Young's moduli was placed on top of the phantom that was relatively either (a) stiffer, having 40KPaYoung's moduli, or (b) softer, having Young's moduli of 10 KPa. The model parameters for phantom were chosen based on typical values encountered for liver tissue [14], while the reference layer was based on the experimentally determined value of a commercially-available material as explained later. The schematic of phantom model geometry, along with the reference layer, is shown in Fig. 1. The model was subjected to a 1% uniaxial compression by loading it from the top while the bottom surface was fixed in the axial direction to prevent rigid body axial translation. Free slip boundary conditions were assumed at lateral faces of the phantom and the reference layer. In addition, the center point of the bottom edge alone was also fixed to prevent rigid body translation in the lateral direction. The Poisson's ratio used for standoff pad and phantom was 0.495.

2.1.2. Ultrasound simulation

Ultrasound simulations were done using Field II software [21]. A linear array transducer was simulated using the parameters listed in Table 1. Pre-compressed RF data were obtained by imaging the phantom containing acoustic scatterers using Conventional Focused

Table 1
Transducer parameters used in field II simulation.

Parameters	Conventional Focused Beamforming (CFB)
Element pitch	0.3 mm
Kerf	0.025 mm
Element height	4 mm
Element width	0.275 mm
Number of elements	128
Number of active elements	64
Center frequency	5 MHz
Sampling frequency	40 MHz
Focal length	20 mm

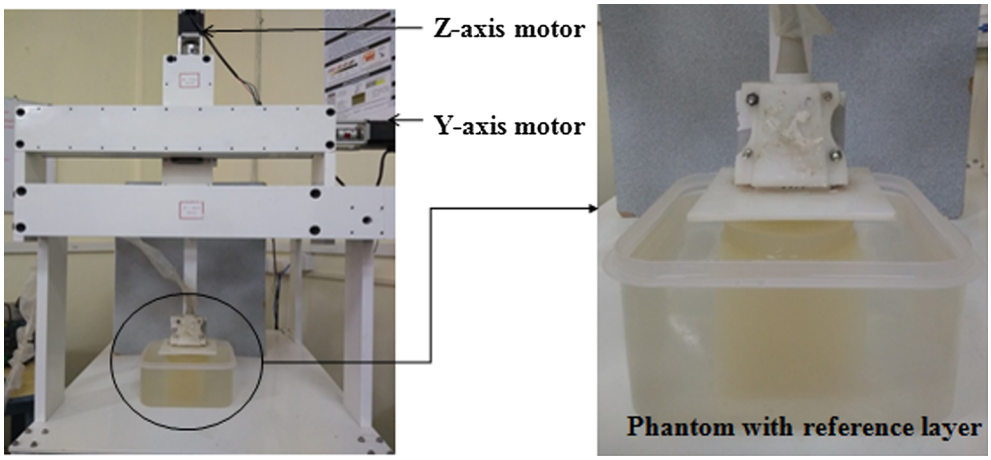

Fig. 2. A photo of the (a) controlled-compression set up that was used for data acquisition, (b) Magnified view of a region (phantom with reference layer) within photo shown in (a).

Beamforming (CFB) technique. Similarly, post compressed RF frame data were obtained after incorporating the displacement data obtained from FEM to the acoustic scatterers positions.

2.1.3. Displacements and strain ratio estimation

A 2-D multilevel block matching algorithm was applied on the pre- and post-compressed RF data to obtain the local tissue displacements [42,30,49,46]. This algorithm selects a reference window in the pre-compressed RF frame data and searches for its closest match in the post-compressed RF frame data. Normalized cross-correlation was used as the similarity measure. In this algorithm, two coarse-level and one fine-level displacement estimations were used. The first-level coarse displacements are obtained from the envelope of the RF frame data, which is decimated by a factor of 4. These displacement estimates are carried forward to serve as a starting point to estimate displacements at the next coarse level. The second-level coarse displacements are obtained similar to the first level, except that the envelope of the RF frame data is now decimated by a factor of 2. In the last level, the finer displacements are estimated from the RF image without any decimation. The search window with 60% overlap was used at all levels. The window length of size 25λ, 5λ, and 3λ and kernel size of dimension (width × length in mm) 1.2 × 7.72, 1.2 × 1.54, and 1.2 × 0.92 were used in first, second, and last level, respectively. Finally, a cosine interpolation in the axial direction and parabolic interpolation in the lateral direction were performed to obtain the sub-sample axial and lateral displacements [8]. These computed axial displacements are then utilized to estimate the axial strain distribution by using least square estimator with a kernel size of 1 mm with an overlap of 0.25 mm [31].

2.1.4. Young's modulus estimation from strain ratio estimate

The unknown modulus of the phantom target is estimated from the phantom-to-reference layer modulus contrast, which is obtained using the following relationship [24,25]:

$$C_m = |2C_s - 1| \quad (1)$$

where C_s is the strain contrast, ($C_s$is the strain ratio between the reference layer and phantom), C_m is the corresponding modulus contrast.

Later, using the known modulus value of the reference material, along with the estimated modulus contrast, we can obtain the unknown target modulus using (2).

$$M_1(unknown) = C_m * M_2(known) \quad (2)$$

Where, M_1 (unknown) – Modulus of phantom target, M_2 (known) – Modulus of reference layer. Note that C_m (from Eq. (1)) used in Eq. (2) captures the strain-contrast to modulus-contrast transfer efficiency.

2.2. Experiments

2.2.1. Reference layer

A 2 cm (Height) × 9 cm (Diameter) aqueous, flexible, disposable ultrasound standoff layer (AQUAFLEX$^{(R)}$, Parker Laboratories, Fairfield, NJ, USA.), which is commercially available was used as a reference layer and is shown in Fig. 2(b). Its modulus value was determined from indentation test using Universal Testing Machine (Jinan TE, China), which is explained in detail in Section 2.3.1.

2.2.2. Phantom preparation

A homogenous tissue-mimicking phantom was used for the experimental validation and which was made using agar-gelatin-water mixtures. In this study, we prepared homogeneous phantoms specifically to correspond to NAFLD, where the liver stiffens homogeneously with the stage of the disease [7,43]. Therefore, we developed homogeneous tissue mimicking material with acoustic and elastic properties that match those of liver tissue values reported in the literature. Thus, the resulting phantom had physiologically realistic Young's modulus and acoustic properties. One can find the detailed procedure for manufacturing this phantom elsewhere [25,16].

For the purposes of this feasibility study phantoms of two different moduli values were only prepared and used. Table 2 presents the gelatin/agar concentration for each of the phantom. The weight of agar and gelatin was mixed with de-ionized water at 80 °C and stirred well until the temperature came down to about 30 °C. Then the mixture was poured into the mold and allowed to cool at 4 °C for approximately 12 h. The phantom prepared was of the dimension 40 mm × 40 mm × 40 mm (width × length × height). Simultaneously, the same molten phantom material was also used to manufacture test samples. The modulus value of the phantom was determined as the modulus of the test samples obtained from indentation testing using Universal Testing Machine (Jinan TE, China), which is explained in detail later in the section.

2.2.3. Data acquisition

The experimental data acquisition was performed using a SONIX TOUCH Q+® scanner (Ultrasonix, Analogic Corporation, Peabody, MA, USA). A linear array transducer (L14-5/38) containing 128-elements, operating at 5 MHz center frequency and a 40 MHz sampling rate were used. The RF data were collected using a single focus at a depth of 25 mm from the phantom surface.

Table 2
Gelatin/agar concentrations of two manufactured phantoms.

Phantom	Agar (% by weight)	Gelatine (% by weight)
Phantom 1	3	5
Phantom 2	3	10

For elastography experiments, the reference layer was placed over the phantom and a compression of 1% was applied on top of the reference layer. The pre- and post-compression RF frame data were acquired and processed using displacement and strain estimation algorithms described in the simulation section earlier. Fig. 2(a) shows the controlled-compression set up that was used for data acquisition. Note that the phantom along with the reference layer was submerged in water during data acquisition.

The above experiment was repeated on the same phantom for five times, but at different elevation planes separated by 5 mm to obtain five independent realizations of RF data for the two different configurations (i.e., configuration 1, reference pad on top of a harder phantom, and configuration 2, reference pad on top of a softer phantom). Here, the modulus of the reference pad does not change from configuration 1 to configuration 2.

2.3. Characterization of elastic and acoustic properties of the prepared phantoms and reference layer

2.3.1. Quasi-static compression test

In order to perform ultrasound stiffness imaging, the prepared samples have to mimic soft tissues in terms of elastic and acoustic properties. Also, we have to know the modulus values of the samples for it to serve as ground truth. Therefore, the elastic properties of the agar-gelatin samples and the reference layers were tested by a computer controlled electro-mechanical UTM (Jinan TE, China) shown in Fig. 3. The 50 kN machine is equipped with an extensometer with 50 mm gauge length. The load cell measures the test load and the deformation of the specimen is measured by an elastometer. Samples were made such that its height is less than twice of its diameter to avoid the buckling effect [34,33]. Quasi-static compression test was performed under displacement controlled mode with a strain rate of 0.5 mm/min up to a maximum of 15% strain. All samples were preconditioned for 5 s and preloaded to 1% of strain (1 mm). We observed from preliminary sample testing that compression beyond 15% strain lead to breakdown of the sample and hence this was set as the upper bound for data acquisition. The slope of the linear portion of the loading curve, which was considered linear up to a maximum of 5% strain, was estimated. Young's modulus was calculated from the slope of the linear portion of the loading curve using the least square fit (Eq. (3)).

$$E = \frac{F/A}{\delta l/l} \tag{3}$$

where E is Young's modulus (KPa), F is the force applied to the sample, A is the original cross-section area through which force is applied (m^2), δl is the change in length (m), l is the original length of the sample (m). Measurements were done for all sets of samples and experiments were repeated for five times on different samples from each set to obtain mean and standard deviation values.

2.3.2. Characterization of acoustic properties

The chosen acoustic parameters were acoustic velocity, attenuation coefficient, and acoustic impedance. Pulse echo method was used to measure the acoustic properties. A5 MHz, 6 mm contact type single-element transducer (V110RM, Olympus NDT) was used for this purpose. The excitation and receiving pulses were controlled by a pulser-receiver (5677, Olympus NDT), which was operated in pulse-echo mode. The received echoes were collected by Oscilloscope at a sampling rate of 50 MHz as shown in Fig. 4. The amplitude (A1 and A2) of echoes from the proximal and distal surface of the samples and time difference between two successive received echoes (t) were measured from the digitized data as shown in Fig. 6. The density of the material was determined as the mass to volume ratio [34]. The dimensions of the phantoms were measured using a vernier caliper (Mitutoyo®, Kawasaki, Japan) and the mass was measured using a digital weighing machine (Sartorius©, Bangalore, India). From these data, the acoustic parameters such as speed of sound (C), attenuation coefficient (A) and acoustic impedance (Z) were calculated for all the prepared phantom samples using standard formulae listed below. This experiment was repeated on five samples of each proportion listed in Table 2.

$$C\left(\frac{\mathrm{m}}{\mathrm{s}}\right) = \frac{2d}{t} \tag{4}$$

$$A\left(\frac{\mathrm{dB}}{\mathrm{cm}}\right) = \frac{1}{2d}20\log\frac{A1}{A2} \tag{5}$$

$$Z\left(\frac{\mathrm{kg}}{\mathrm{m^2 s}}\right) = \rho C \tag{6}$$

where d is the height of the sample in meters.

The speed of sound, attenuation and impedance were measured for both the phantoms and calibration layer in order to verify that the samples prepared for the experiments have acoustic properties that lie within the range reported in the literature for liver tissue [6,34,33].

2.3.3. Reliability and stability of reference pad

The reliability and stability of the reference pad were studied using the modulus value measured at 30 days-interval for over a period of 4 months. The phantoms were stored in a refrigerator at 15 °C and new reference pads from the batch were used at each of the time points. The

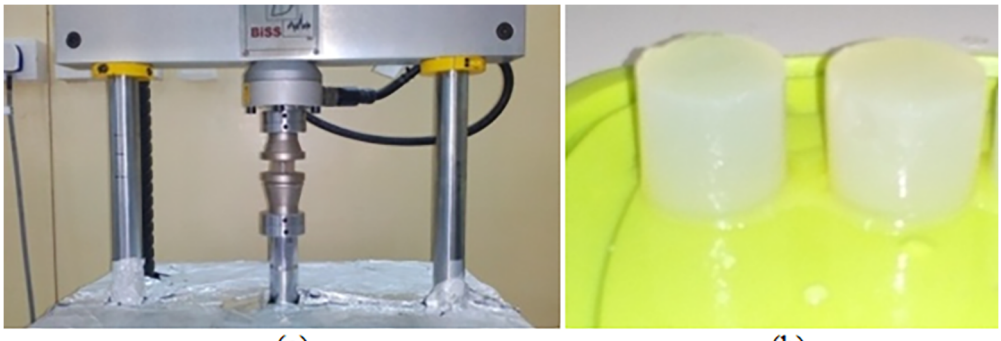

Fig. 3. A photo showing the (a) Universal testing machine used for characterization of elastic properties, and (b) Samples that were characterized for elastic properties.

Fig. 4. A photo of the experimental setup used for measuring and characterizing the acoustic properties of the test samples.

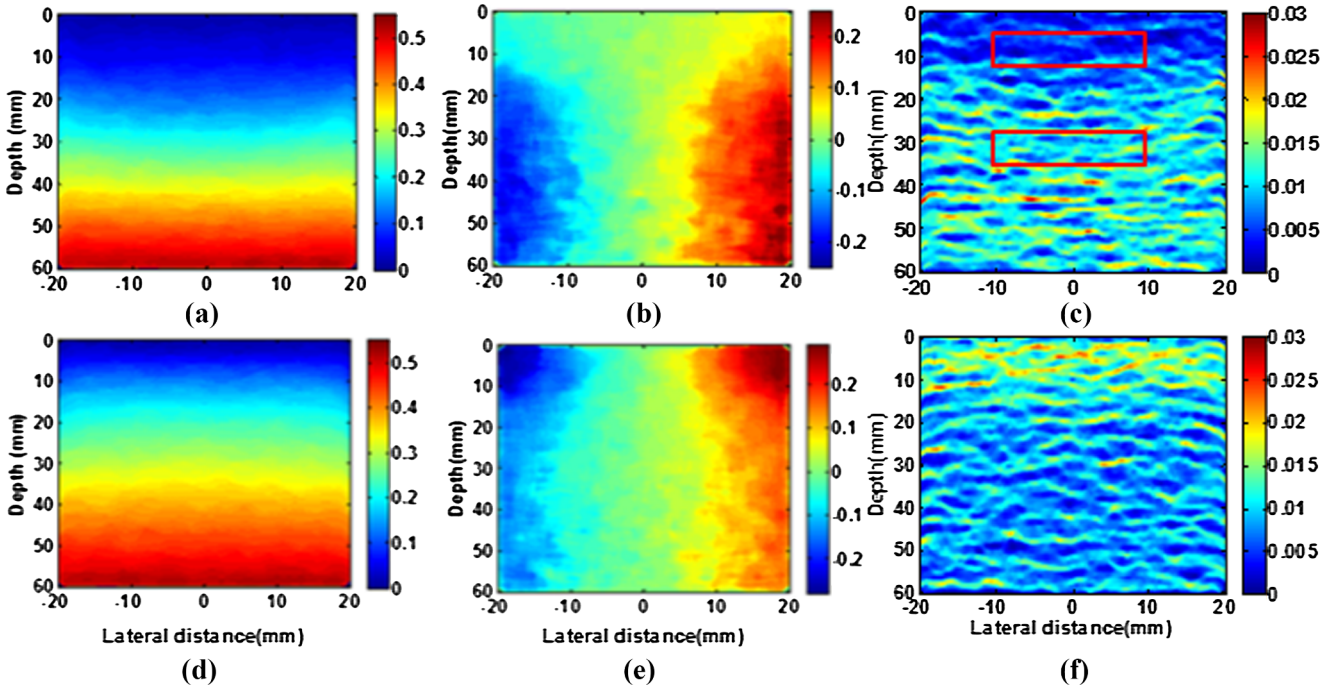

Fig. 5. Images obtained from simulated ultrasound data for configuration 1 (Reference layer = 20 KPa, Phantom = 10 KPa) (a) axial displacements, (b) lateral displacements, and (c) axial strain and configuration 2 (Reference layer = 20 KPa, Phantom = 40 KPa), (d) axial displacements, (e) lateral displacements, and (f) axial strain.

modulus value was determined by indentation testing using Universal Testing Machine (Jinan TE, China), similar to how it was done for phantom samples described in the earlier Section 2.3.1.

3. Results

3.1. Simulation results

3.1.1. Ultrasound elastography simulation

Images of axial displacements, lateral displacements, and axial strain estimated from the simulated ultrasound data are shown in Fig. 5. In these images, the reference layer spans 20 mm from the top and the remaining region represents the phantom. Notice the conspicuous changes in the lateral displacements, which show that the reference layer undergoes less displacement compared to the underlying phantom when the reference layer is stiffer than the phantom. Further, the axial strain image shows that the phantom undergoes more strain compared to the reference layer. As one would expect, the exact opposite, i.e., phantom undergoing less strain than the reference layer and the lateral displacements being more in the reference layer than in the phantom, is observed in configuration 2.

Table 3
The mean and standard deviation values of elastic properties obtained in simulations.

Configuration	Measured strain ratio (C_s)	Estimated (KPa)	Ground truth (KPa)
1	0.76 ± 0.05	10.43 ± 1.45	10
2	1.52 ± 0.08	40.81 ± 4.20	40

The modulus value of the phantom estimated from the elastogram and the ground truth set in FEM are listed and compared in Table 3. Simulation results suggest that the modulus value of the phantom can be estimated from elastogram within an error of 6%.

3.2. Experiment results

3.2.1. Characterization of acoustic properties of reference layer and phantom samples

The mean and standard deviation values for the different acoustic parameters measured are presented in Table 4. It can be observed that

Table 4
The mean and standard deviation values for acoustic properties of the prepared samples and reference layer.

Sl. no	Parameter	Sample 1 (phantom)	Sample 2 (reference pad)	Literature
1	Speed of sound [ms^{-1}]	1580 ± 24	1670 ± 36	1564–1700
2	Acoustic impedance [kg m^2s^{-1}](*10^6)	1.642 ± 0.254	1.710 ± 0.012	1.64–1.71
3	Attenuation coefficient (dB cm^{-1} MHz^{-1})	0.891 ± 0.136	0.658 ± 0.346	0.700–0.900

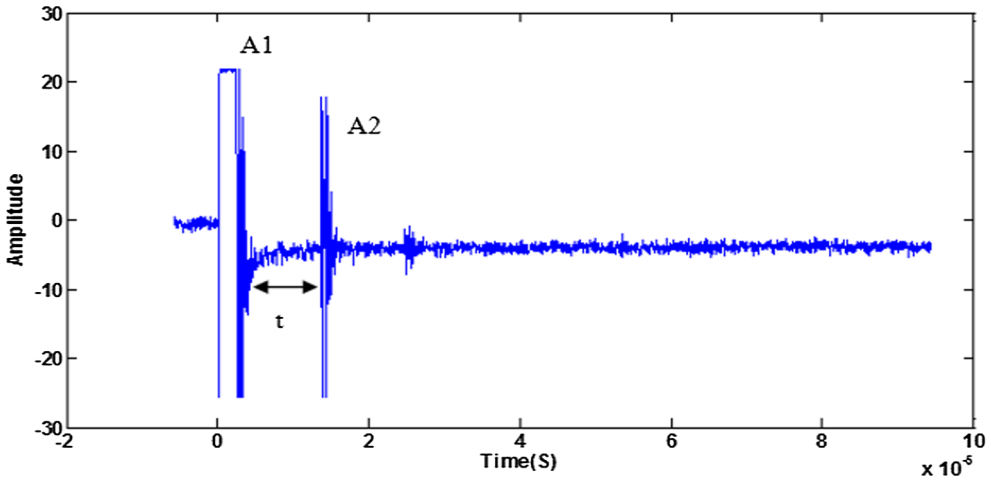

Fig. 6. Plot of the A-line from a test sample used in the measurement of acoustic properties with markings showing A1 and A2, the echoes from the proximal and distal surface of the sample, respectively.

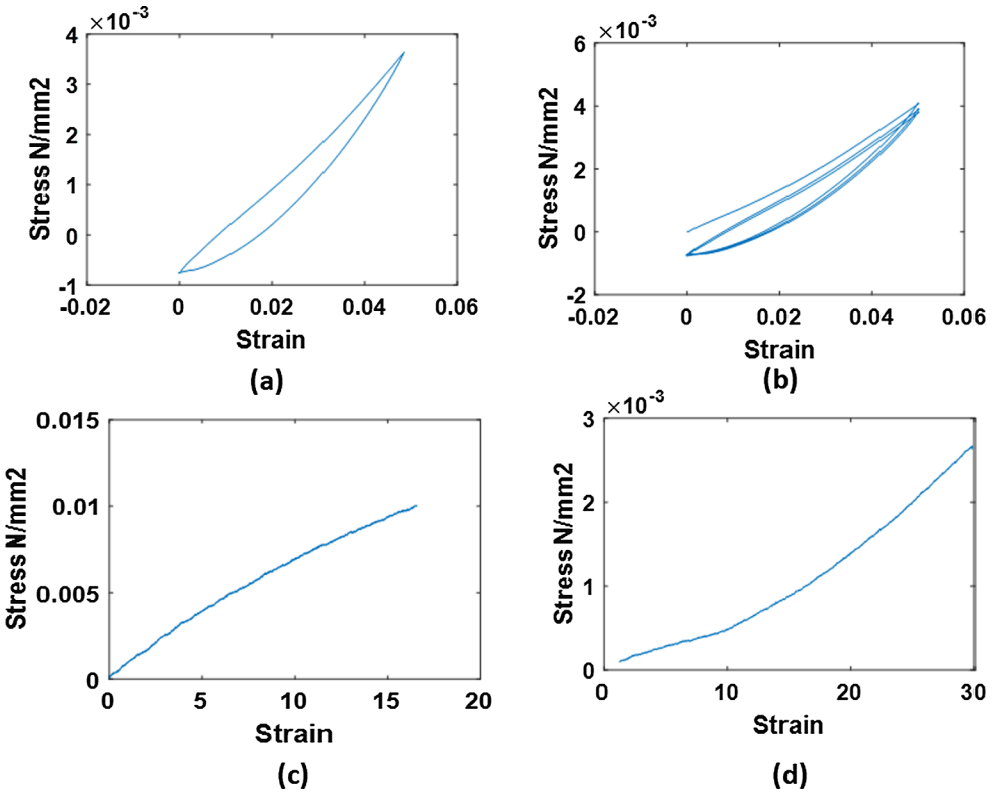

Fig. 7. Plots of (a) loading and unloading stress-strain curve of phantom sample (b) 3 cycles of load-unload stress-strain curve for reference layer sample. Notice that the curve has hysteresis indicating the samples are actually viscoelastic in nature. For elastic characterization, the loading part alone was considered. Plots of the stress-strain loading curve for the (c) phantom samples and (d) reference layer.

the phantom samples prepared for the experiments have acoustic properties that lie within the range reported in the literature for liver tissue [6,34,33]. Having characterized the elastic and acoustic properties of homogeneous samples, a composite phantom was used for ultrasound elastography imaging. An example A-line obtained from a test sample to measure its acoustic property is shown in Fig. 6.

3.2.2. Characterization of elastic properties using UTM-stress-strain curve:
Fig. 7 shows the typical stress-strain curve obtained during compression testing of the samples from which the modulus value was estimated for each sample. The moduli values for the two different phantoms and the reference pad obtained from UTM testing are listed in Table 5.

Table 5
Elastic properties of the samples from UTM.

	Modulus from compression testing (KPa)
Reference layer	20 ± 1.80
Phantom 1	10.25 ± 1.84
Phantom 2	40.37 ± 1.26

3.2.3. Ultrasound elastography experiment

Fig. 8 shows the axial displacement image, lateral displacement image, and axial strain elastogram obtained from experiment for the two different configurations. Although the Aquaflex® standoff pads are hypoechoic, the displacement, strain and modulus calculations used in the phantom experiments are the exact same as that done in simulations. Additional details on strain estimation in the standoff pads are provided in Appendix A. The lateral displacements and axial strain distribution show similar behavior as noted in simulations, i.e., the reference layer undergoes less (or more) lateral displacement compared to the phantom and the phantom undergoes more (or less) axial strain compared to the reference layer, depending on the configuration. The unknown modulus value of the phantom was estimated and it was compared with the modulus values of phantom samples measured using UTM experiments. The results are shown in Table 6. Results from the experiments suggest that the unknown modulus value of the phantom was estimated within an error of 11%.

3.2.4. Evaluation of the proposed method using a commercially-available elastography option

In the earlier sections, Young's modulus was estimated from the strain-ratio values obtained offline using in-house developed algorithms. Here, we compare Young's modulus obtained from strain ratio measured using SONIX TOUCH Q+® scanner (Ultrasonix, Analogic Corporation, Peabody, MA, USA). The imaging was done with a linear array transducer (L14-5/38) operating at 5 MHz center frequency. The RoI was placed on the reference layer and the phantom, respectively, for obtaining the strain ratio as shown in Fig. 9. Form the strain ratio, unknown phantom modulus was calculated as described earlier in Section 2.1.4. The results are tabulated in Table 7. The results seem to be consistent with the offline simulation and experimental results obtained earlier.

3.2.5. Young's modulus vs age of reference layer

The Young's modulus value of the reference gel-pad measured at different times is plotted in Fig. 10. The error bar around each point represents standard deviation from five different samples from the same batch. The elastic modulus values of the reference pad samples were found to be 20 KPa on an average and this value was used as a common reference in estimating unknown modulus of phantom material from the strain ratio. It can be noted from Fig. 8 that the reference pad had stable Young modulus value over the period of first three months.

4. Discussion and conclusions

In this work, we characterized and reported Young's modulus value of a commercially available material that can act as a reference layer for liver elastography. Further, we also incorporated the contrast transfer efficiency paradigm while estimating the modulus contrast from estimated strain contrast. The present study investigated the feasibility of quantifying the stiffness of underlying tissue in simulations and *in vitro* phantom experiments. The results suggest that quasi-static elastography with a calibrated reference layer can be used for estimating the unknown tissue stiffness within an error of 6% in simulations and 11% in experiments.

Also, the results form Tables 6 and 7 confirmed the translational capability of the proposed method to work with existing commercially-available ultrasound scanner having elastography option. A further analysis of the intra-observer and inter-observer repeatability of the proposed quantitative technique is reported in Appendix A. Other quantitative stiffness measurement methods, such as shear wave based techniques for assessment of liver stiffness are still under investigation. Moreover, further work is needed as there are some reports that show

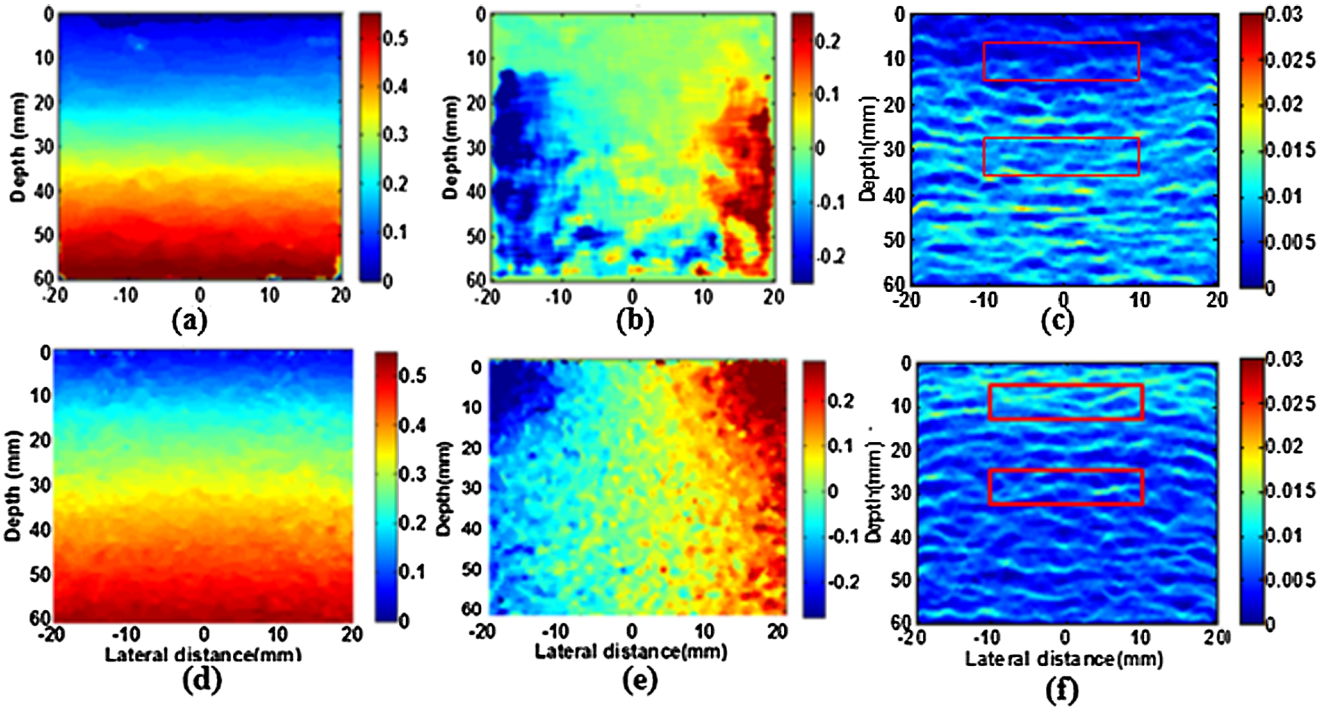

Fig. 8. Images obtained from elastography experiments for configuration 1 (Reference layer = 20 KPa, Phantom = 10 KPa) (a) axial displacements, (b) lateral displacements, and (c) axial strain and Configuration 2 (Reference layer = 20 KPa, Phantom = 40 KPa), (d) axial displacements, (e) lateral displacements, and (f) axial strain.

Table 6
The mean and standard deviation values for strain ratio and unknown sample modulus value.

Configuration	Measured strain ratio (C_s)	Estimated modulus (KPa)	Modulus value from UTM testing (KPa)
1	0.73 ± 0.07	9.21 ± 2.23	10.25 ± 1.84
2	1.48 ± 0.12	39.24 ± 4.10	40.82 ± 3.75

Table 7
The mean and standard deviation values for strain ratio and unknown sample modulus value.

Configurations	Measured strain ratio from the ultrasound scanner	Modulus of unknown phantom (KPa)	Modulus value from UTM testing (KPa)
1	0.77 ± 0.15	10.80 ± 1.20	10.25 ± 1.84
2	1.58 ± 0.21	41.24 ± 3.79	40.82 ± 3.75

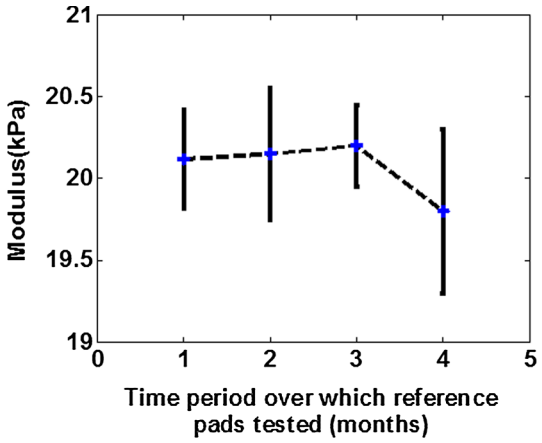

Fig. 10. Plot of the measured Young's modulus value of the reference layer over the age of the reference pad from the date of opening the box.

measurement variation from scanner to scanner [11]. Furthermore, these methods require specific and expensive systems. One of the major advantages of the proposed approach is that it can be easily used with standard ultrasound scanner having elastography software and a calibrated reference layer that is commercially available.

In the approach proposed here only the axial-strain distributions i.e., strain along the insonification direction is imaged and used, while lateral (perpendicular to the beam propagation direction and scan plane) displacements are not used. Although it was not explicitly stated in the earlier sections, one could easily produce a modulus image simply by extending the proposed approach to a pixel-sized ROI. One such modulus image of the two different phantoms from experiments is shown in Fig. 11.

Nevertheless, there are several methods reported in the literature that seeks to estimate the modulus image from displacement and strain data from axial and lateral directions using inverse reconstruction techniques [12]. It is possible that some of the simple inverse reconstruction methods that are real-time can be adopted for the case considered. In general, the accuracy, robustness, and speed of inverse reconstruction improve with better quality input estimates of axial and lateral displacement data [3,2,36]. Recently, there have been many methods proposed to obtain better quality lateral displacement estimates in elastography [41,32,22,31,28,45,17,10,29,27,48,38]. We are currently investigating on combining the reference layer methodology and inverse reconstruction approach having access to better-quality lateral displacement estimates, and compare it with the simple approach proposed here.

Regarding the choice of material for the reference layer, we initially tried using phantoms made of agar/gelatin mixtures. However, the stability and shelf-life of the in-house manufactured pad were found to be very limited. Therefore, a commercially available standoff pad was tested for its potential to serve as the reference material, which was also suggested recently by [47]. The results suggest that their Young's modulus value changed very little over the 4-month period of testing. The test was performed over this period from the date of opening the box. Even after this time, there were about 9-months left before the expiry date listed on the box label. Nevertheless, one has to take care that the standoff pad is stored and maintained properly. If the mechanical properties of the pad changes, it will greatly affect our results because only the calibrated modulus value of the reference pad is considered for the estimation of the unknown modulus value. Also, a perfect reference material would have no attenuation, speed of sound would be around 1540 m/s, and the stiffness should not be too different from that of the target organ (e.g., Liver). The thickness of the standoff layer may be around 20 mm seems a reasonable choice considering the trade-off between increased depth of imaging viz-a-viz minimizing the reference layer-tissue boundary effect. It must be recognized that the

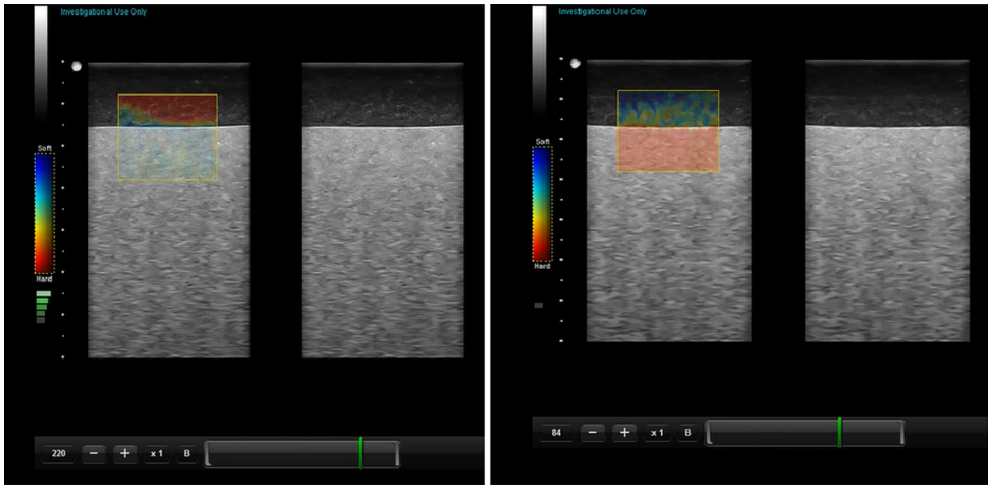

(a) (b)

Fig. 9. Screen shot of elastography imaging using SonixTouchQ + ultrasound scanner for (a) configuration 1 (Reference layer = 20 KPa, Phantom = 10 KPa), (b) configuration 2 (Reference layer = 20 KPa, Phantom = 40 KPa).

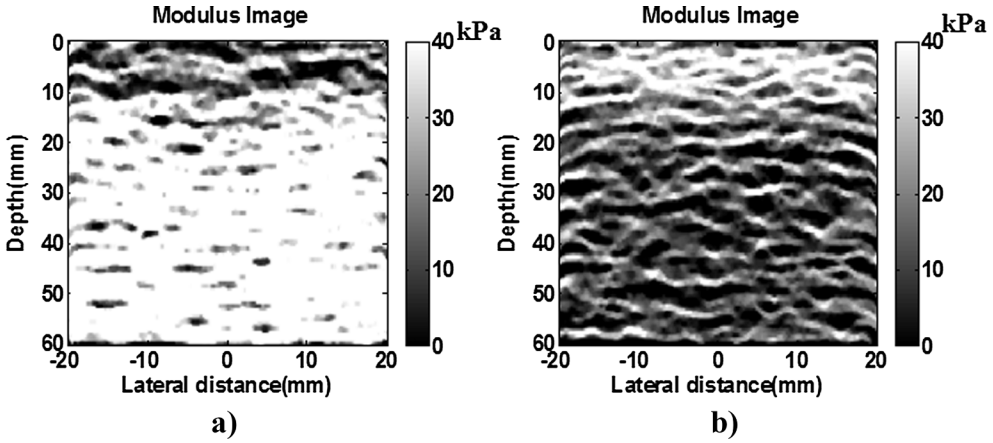

Fig. 11. Modulus images obtained from elastography experiments for (a) configuration 1 (Reference layer = 20 KPa, Phantom = 40 KPa), (b) configuration 2 (Reference layer = 20 KPa, Phantom = 10 KPa).

data from the stand-off pad was beamformed using a speed of sound of 1540 m/s and not the estimated value from experiments as all scanners are calibrated for 1540 m/s. Ofcourse, with newer adaptive beamformers the quality of RF data is corrected for these aberrations. Therefore, if these are incorporated then the results may be even better.

In addition, regarding the boundary condition used in FEM, it must be noted that a thin layer of ultrasound gel can be applied between transducer-standoff pad interface as well as standoff pad-phantom interface and therefore these were modeled as free-slip boundary condition. However, even when this boundary condition is not completely satisfied and some non-slip/or high friction condition is present between the US transducer and the standoff pad, this was found (not reported here) to have a very little effect on the estimated strain ratio values. This was also due to the choice of the RoI, which was done in such a way that the boundary condition will have little influence on the strain contrast measurement (e.g., see Figs. 5 and 8 where RoI is shown).

In summary, a method to make quasi-static ultrasound elastography Quantitative using a reference layer was investigated. The feasibility of this approach was demonstrated using simulations and phantom experiments *in vitro*. The Young's modulus estimated from elastography in simulation and experiment was compared against the corresponding ground-truth modulus value obtained from COMSOL and UTM results, respectively. The results suggest that it is possible to estimate the compressive elastic modulus of the underlying phantom using quasi-static ultrasound elastography and a calibrated reference material to within 6% and 11%in simulation and experiments, respectively.

Declaration of conflicting interests

The author(s) declared no potential conflicts of interest with respect to the research, authorship, and/or publication of this article.

Acknowledgments

Mr. Sathiyamoorthy would like to thank MHRD, Govt. of India for supporting through Half-Time Research Assistantship. The authors would like to thank Dr. A. Arockiarajan and Dr. Pijush Ghosh of IIT Madras for providing the facilities to conduct indentation experiments.

Appendix A. Displacement tracking and strain estimation in reference standoff pad region

Aquaflex® standoff pads are hypoechoic and almost no speckle is visible in the usual display. However, if the B-mode image in Fig. A1 is observed carefully one can notice speckle in the stand-off pad region, although very weak. Initially, we estimated the overall displacement by tracking only the standoff pad-phantom interface as shown in the figure below and estimated the strain from the fundamental definition, Strain = $\delta l/l$.

However, it was noticed that although the amplitude of RF signal from the standoff pad was weak, the motion tracking algorithms and strain estimation were not affected. An example B-mode image of a phantom with a standoff pad at the top and one RF A-line from the center is shown below in Fig. A2.

As shown in Fig. 9 earlier one can notice strain contrast in the elastograms displayed by Sonix machine as well, while the B-mode shows the standoff pad as a hypoechoic region. In addition, the advantage of performing motion tracking in the standoff region is that it allows for easy visual differentiation of the relative stiffness of the reference layer region (0–20 mm) by observing the lateral displacement image (For e.g., Fig. 8b and e).

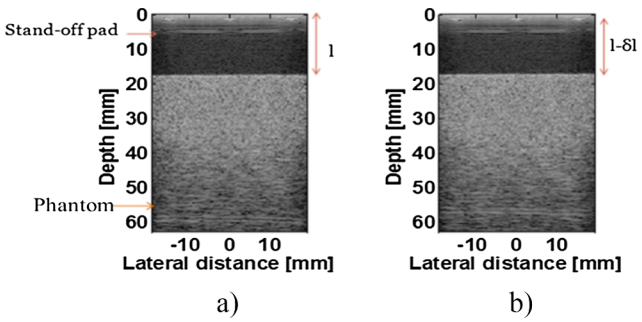

Fig. A1. Illustrates the lack of prominent speckle signal in the standoff pad in the B-mode images (a) pre-compression and (b) post-compression, when displayed in 60 dB dynamic range.

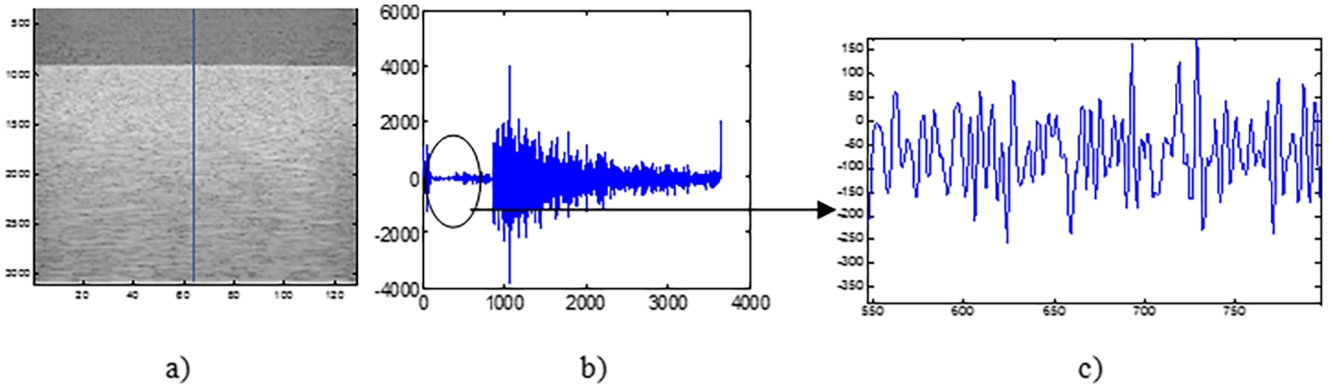

Fig. A2. An example case to illustrate the signal amplitude from the standoff pad region is shown in relation to (a) B-mode image display having standoff pad, b) complete central RF A-line and c) A magnified view of a region within plot shown in (b).

Appendix B. An analysis of intra-observer and inter-observer repeatability of the proposed quantitative technique

In order to assess the intra-observer and inter-observer variability in the estimated Young's modulus value using the proposed quantitative technique, a free-hand elastography study on phantoms was performed. Two operators were instructed to perform gentle compression and relaxation in freehand using L5-14 transducer probe working with SONIX TOUCH Q+® scanner (Ultrasonix, Analogic Corporation, Peabody, MA, USA). The elsatography mode was ON and the operators had real-time strain elastogram displayed on the screen for feedback. The operators performed this exercise for the two different configurations (stiffer phantom and softer phantom, respectively). The cine-loop of RF frame data was saved and processed as described earlier. The variation of strain contrast and estimated modulus value for each frame within the cine-loop was obtained from each operator data to understand the intra-operator and inter-operator variability. The cine-loop consisted of 20 strain elastograms, from which the mean and standard deviations are calculated and reported in Tables B1 and B2.

The results suggest that intra-observer variability when performing the experiment in freehand is slightly more for Operator 1 in configuration 2 (~24%), while it is within 15% for all other cases. Further, the error between estimated modulus values by each operator against the expected ground truth is within 5% for configuration 1, and as high as about 13% for operator 2 in configuration 2. Although this analysis is preliminary and is only on phantoms, it is more realistic than results in Table 7 as these are obtained using freehand compression. The inter- and intra-observer variability can be reduced further by using assisted-freehand compression devices [1], which is currently under investigation.

Table B1
Strain ratio and estimated modulus measurements for configuration 1.

Sl. No	Parameter	Operator 1	Operator 2
1.	Strain ratio	1.52 ± 0.18	1.55 ± 0.16
2.	Young's Modulus (KPa)	40.80 ± 4.50	42 ± 6.40

Table B2
Strain ratio and estimated modulus measurements for configuration 2.

Sl. No	Parameter	Operator 1	Operator 2
1.	Strain ratio	0.72 ± 0.09	0.79 ± 0.15
2.	Young's modulus (KPa)	9.18 ± 2.23	11.60 ± 1.25

References

[1] V. Abilash, A.K. Thittai, Development of a compact hand-held device for use in quasi-static elastography: a preliminary study on tissue-mimicking phantom, in: Proceedings of the 16th International Tissue Elasticity Conference, Avignon, France, px, 2018.
[2] U. Albocher, A.A. Oberai, P.E. Barbone, I. Harari, Adjoint-weighted equation for inverse problems of incompressible plane-stress elasticity, Comput. Methods Appl. Mech. Eng. 198 (30–32) (2009) 2412–2420.
[3] O.A. Babaniyi, A.A. Oberai, P.E. Barbone, Recovering vector displacement estimates in quasistatic elastography using sparse relaxation of the momentum equation, Inverse Prob. Sci. Eng. 25 (3) (2017) 326–362.
[4] S. Bellentani, F. Scaglioni, M. Marino, G. Bedogni, Epidemiology of non-alcoholic fatty liver disease, Dig. Dis. 28 (1) (2010) 155–161.
[5] J. Bercoff, M. Tanter, M. Fink, Supersonic shear imaging: a new technique for soft tissue elasticity mapping, IEEE Trans. Ultrason. Ferroelectr. Freq. Control 51 (4) (2004) 396–409.
[6] P.L. Carson, Biomedical ultrasonics. By PNT Wells, Ph. D., Academic Press, Inc. London, copyright 1977, J. Clin. Ultrasound (1978) 635.
[7] L. Castera, X. Forns, A. Alberti, Non-invasive evaluation of liver fibrosis using transient elastography, J. Hepatol. 48 (5) (2008) 835–847.
[8] I. Céspedes, Y. Huang, J. Ophir, S. Spratt, Methods for estimation of subsample time delays of digitized echo signals, Ultrason. Imaging 17 (2) (1995) 142–171.
[9] L. Chen, L.K. Low, J.O. DeLancey, J.A. Ashton-Miller, In vivo estimation of perineal body properties using ultrasound quasistatic elastography in nulliparous women, J. Biomech. 48 (9) (2015) 1575–1579.
[10] X. Chen, M.J. Zohdy, S.Y. Emelianov, M. O'Donnell, Lateral speckle tracking using synthetic lateral phase, IEEE Trans. Ultrason. Ferroelectr. Freq. Control 51 (5) (2004) 540–550.
[11] S. Colombo, M. Buonocore, A. Del Poggio, C. Jamoletti, S. Elia, M. Mattiello, D. Zabbialini, P. Del Poggio, Head-to-head comparison of transient elastography (TE), real-time tissue elastography (RTE), and acoustic radiation force impulse (ARFI) imaging in the diagnosis of liver fibrosis, J. Gastroenterol. 47 (4) (2012) 461–469.
[12] M.M. Doyley, Model-based elastography: a survey of approaches to the inverse elasticity problem, Phys. Med. Biol. 57 (3) (2012) R35.
[13] J. Foucher, E. Chanteloup, J. Vergniol, L. Castera, B. Le Bail, X. Adhoute, J. Bertet, P. Couzigou, V. de Ledinghen, Diagnosis of cirrhosis by transient elastography (FibroScan): a prospective study, Gut 55 (3) (2006) 403–408.

[14] N. Frulio, H. Trillaud, Ultrasound elastography in liver, Diagnostic Intervent. Imag. 94 (5) (2013) 515–534.
[15] Z.D. Goodman, Grading and staging systems for inflammation and fibrosis in chronic liver diseases, J. Hepatol. 47 (4) (2007) 598–607.
[16] T.J. Hall, M. Bilgen, M.F. Insana, T.A. Krouskop, Phantom materials for elastography, IEEE Trans. Ultrason. Ferroelectr. Freq. Control 44 (6) (1997) 1355–1365.
[17] H.H.G. Hansen, R.G.P. Lopata, T. Idzenga, C.L. de Korte, Full 2D displacement vector and strain tensor estimation for superficial tissue using beam-steered ultrasound imaging, Phys. Med. Biol. 55 (11) (2010) 3201.
[18] H.S. Hashemi, S. Fallone, M. Boily, A. Towers, R.D. Kilgour, H. Rivaz, Ultrasound elastography of breast cancer-related lymphedema, in: 2018 IEEE 15th International Symposium on Biomedical Imaging (ISBI 2018), Washington, DC, 2018, pp. 1491–1495. doi: 10.1109/ISBI.2018.8363855.
[19] L. Hee, D. Liao, P. Sandager, H. Gregersen, N. Uldbjerg, Cervical stiffness evaluated in vivo by endoflip in pregnant women, PLoS One 9 (3) (2014) e91121.
[20] L. Hee, C.K. Rasmussen, J.M. Schlütter, P. Sandager, N. Uldbjerg, Quantitative sonoelastography of the uterine cervix prior to induction of labor as a predictor of cervical dilation time, Acta Obstet. Gynecol. Scand. 93 (7) (2014) 684–690.
[21] J.A. Jensen, et al., Paper presented at the 10th Nordic-Baltic Conference on Biomedical Imaging : Field : A Program for Simulating Ultrasound Systems Field: A Program for Simulating Ultrasound Systems 34 (1996) 351–353.
[22] J.A. Jensen, S.I. Nikolov, K.L. Gammelmark, M.H. Pedersen, Synthetic aperture ultrasound imaging, Ultrasonics 44 (2006) e5–e15.
[23] W.K. Jeong, H.K. Lim, H.K. Lee, J.M. Jo, Y. Kim, Principles and clinical application of ultrasound elastography for diffuse liver disease, Ultrasonography 33 (3) (2014) 149.
[24] F. Kallel, M. Bertrand, J. Ophir, Fundamental limitations on the contrast-transfer efficiency in elastography: an analytic study, Ultrasound Med. Biol. 22 (4) (1996) 463–470.
[25] F. Kallel, C.D. Prihoda, J. Ophir, Contrast-transfer efficiency for continuously varying tissue moduli: simulation and phantom validation, Ultrasound Med. Biol. 27 (8) (2001) 1115–1125.
[26] R. Kishimoto, M. Suga, A. Koyama, T. Omatsu, Y. Tachibana, D.K. Ebner, T. Obata, Measuring shear-wave speed with point shear-wave elastography and MR elastography: a phantom study, BMJ Open 7 (1) (2017) e013925.
[27] S. Korukonda, M.M. Doyley, Estimating axial and lateral strain using a synthetic aperture elastographic imaging system, Ultrasound Med. Biol. 37 (11) (2011) 1893–1908.
[28] A. Kothawala, S. Chandramoorthi, N.R.K. Reddy, A.K. Thittai, Spatial compounding technique to obtain rotation elastogram: a feasibility study, Ultrasound Med. Biol. 43 (6) (2017) 1290–1301.
[29] H. Liebgott, A. Basarab, P. Gueth, D. Friboulet, P. Delachartre, Transverse oscillations for tissue motion estimation, Ultrasonics 50 (6) (2010) 548–555.
[30] R.G. Lopata, M.M. Nillesen, H.H. Hansen, I.H. Gerrits, J.M. Thijssen, C.L. De Korte, Performance evaluation of methods for two-dimensional displacement and strain estimation using ultrasound radio frequency data, Ultrasound Med. Biol. 35 (5) (2009) 796–812.
[31] B. Lokesh, B.R. Chintada, A.K. Thittai, Rotation elastogram estimation using synthetic transmit-aperture technique: a feasibility study, Ultrason. Imaging 39 (3) (2017) 189–204.
[32] J. Luo, E.E. Konofagou, Effects of various parameters on lateral displacement estimation in ultrasound elastography, Ultrasound Med. Biol. 35 (8) (2009) 1352–1366.
[33] K. Manickam, R.R. Machireddy, S. Seshadri, Characterization of biomechanical properties of agar based tissue mimicking phantoms for ultrasound stiffness imaging techniques, J. Mech. Behav. Biomed. Mater. 35 (2014) 132–143.
[34] K. Manickam, R.R. Machireddy, S. Seshadri, Study of ultrasound stiffness imaging methods using tissue mimicking phantoms, Ultrasonics 54 (2) (2014) 621–631.
[35] S. Mueller, L. Sandrin, Liver stiffness: a novel parameter for the diagnosis of liver disease, Hepatic Med.: Evid. Res. 2 (2010) 49.
[36] X. Pan, K. Liu, J. Bai, J. Luo, A regularization-free elasticity reconstruction method for ultrasound elastography with freehand scan, Biomed. Eng. Online 13 (1) (2014) 132.
[37] N. Redhu, D. Rastogi, A. Yadav, S. Hariprasad, Z. Jigar, S. Tripathi, D. Chawla, Ultrasound elastography–Review, Curr. Med. Res. Pract. 5 (2) (2015) 67–71.
[38] M. Rao, Q. Chen, H. Shi, T. Varghese, E.L. Madsen, J.A. Zagzebski, T.A. Wilson, Normal and shear strain estimation using beam steering on linear-array transducers, Ultrasound Med. Biol. 33 (1) (2007) 57–66.
[39] E. Rossi, L.A. Adams, M. Bulsara, G.P. Jeffrey, Assessing liver fibrosis with serum marker models, Clin. Biochem. Rev. 28 (1) (2007) 3.
[40] L. Sandrin, C. Fournier, V. Miette, G. Millonig, S. Mueller, Fibroscan® in hepatology: a clinically-validated tool using vibration-controlled transient elastography, Ultrasonics Symposium (IUS), 2009 IEEE International, IEEE, 2009, pp. 1431–1434.
[41] S. Selladurai, A.K. Thittai, Strategies to obtain subpitch precision in lateral motion estimation in ultrasound elastography, IEEE Trans. Ultrason. Ferroelectr. Freq. Control 65 (3) (2018) 448–456.
[42] H. Shi, T. Varghese, Two-dimensional multi-level strain estimation for discontinuous tissue, Phys. Med. Biol. 52 (2) (2007) 389.
[43] P. Stål, Liver fibrosis in non-alcoholic fatty liver disease-diagnostic challenge with prognostic significance, World J. Gastroenterol.: WJG 21 (39) (2015) 11077.
[44] K.T. Suk, S.K. Baik, J.H. Yoon, J.Y. Cheong, Y.H. Paik, C.H. Lee, Y.S. Kim, J.W. Lee, D.J. Kim, S.W. Cho, S.G. Hwang, Revision and update on clinical practice guideline for liver cirrhosis, Korean J. Hepatol. 18 (1) (2012) 1.
[45] U. Techavipoo, Q. Chen, T. Varghese, J.A. Zagzebski, Estimation of displacement vectors and strain tensors in elastography using angular insonifications, IEEE Trans. Med. Imaging 23 (12) (2004) 1479–1489.
[46] A.K. Thittai, B. Galaz, J. Ophir, Axial-shear strain distributions in an elliptical inclusion model: experimental validation and in vivo examples with implications to breast tumor classification, Ultrasound Med. Biol. 36 (5) (2010) 814–820.
[47] Y. Yamamoto, S. Yamaguchi, T. Sasho, T. Fukawa, Y. Akatsu, K. Nagashima, K. Takahashi, Quantitative ultrasound elastography with an acoustic coupler for achilles tendon elasticity, J. Ultrasound Med. 35 (1) (2016) 159–166.
[48] S.S. Yengul, O.A. Babaniyi, F.C. Meral, B. Madore, P.E. Barbone, Improving ultrasound-based estimates of vector displacement fields in elastography applications, J. Acoust. Soc. Am. 135 (4) (2014) 2156–2156.
[49] Y. Zhu, T.J. Hall, A modified block matching method for real-time freehand strain imaging, Ultrason. Imaging 24 (3) (2002) 161–176.